Thermo-mechanical properties of polystyrene-based shape memory nanocomposites†

B. Xu,[a] Y. Q. Fu,*[a] M. Ahmad,[b] J. K. Luo,[b] W. M. Huang,[c] A. Kraft,[a] R. Reuben,[a] Y. T. Pei,[d] Z. G. Chen[d] and J. Th. M. De Hosson[d]

Received 6th November 2009, Accepted 11th December 2009
First published as an Advance Article on the web 29th January 2010
DOI: 10.1039/b923238a

Shape memory nanocomposites were fabricated using chemically cross-linked polystyrene (PS) copolymer as a matrix and different nanofillers (including alumina, silica and clay) as the reinforcing agents. Their thermo-mechanical properties and shape memory effects were characterized. Experimental results revealed that the nanofillers provide significant reinforcement of the PS, and the nanocomposites exhibit better thermal and mechanical properties, including shape memory properties, than unreinforced PS. Both experimental and theoretical analyses have shown that the rod-shaped clay nanofillers offer better reinforcement than spherical nanoparticles, because of their high aspect ratio and ability to reinforce in multiple directions.

1. Introduction

After large deformations followed by a period at low temperature, a shape memory polymer (SMP) can recover its original shape, triggered by external stimuli such as heat,[1] electric fields,[2] magnetic fields[3] and light.[4] The basic shape memory mechanism is based on reversible energy conversion in polymer chain movement. For example, thermal triggering can occur with a transition temperature equal to the melting temperature or glass transition temperature, depending on the nature of the shape memory polymer.[5] SMPs offer a much higher degree of deformation and a wider scope of mechanical properties than shape memory alloys (SMAs), in addition to their inherent advantages of cheapness, biocompatibility, light weight, and easy processing.[6] However, the low strength of polymers limits their applications. To overcome this disadvantage, a range of nanofillers have been introduced into SMP matrices, and nanocomposites made from dispersed particles of sizes smaller than 100 nm have been shown to improve the strength and elastic modulus of the matrix.[7,8] Polystyrene (PS) has been widely used as the hard segment in copolymers for nanocomposite design and applications because of its low cost compared to other strong polymers such as PMMA, polyurethane, and polycarbonate. Although some studies have been carried out on the shape memory properties of PS-based SMPs,[9,10] there has been no comprehensive study of the underpinning physical and mechanical enhancement mechanisms of PS-based shape memory nanocomposites. This paper presents a systematic investigation of the PS-based shape memory nanocomposites with different types of nanofillers. A theoretical analysis of the observed mechanical enhancement of the nanocomposite SMPs is also performed.

2. Experimental

The matrix was prepared for a styrene-based prepolymer with benzyl peroxide (BPO) curing agent (CRG Company, USA). The nanofillers were attapulgite clay, silica (SiO_2, average grain size ~15 nm) and alumina (Al_2O_3, average grain size ~80 nm). The heat treatment of the attapulgite clay powder (850 °C for 2 h) was reported in ref. 11. All of the nanofillers were dried in an oven at 120 °C for 24 h to remove moisture. They were then mixed with the prepolymer for 15 min by stirring at a rotation speed of 1000 rpm, followed by treatment for 45 min with ultrasonic mixer. The curing agent was then added and the mixture again stirred at 1000 rpm for 15 min, followed by ultrasonic agitation for 45 min. Samples were prepared by casting the mixture into PTFE moulds and baking at 75 °C for 36 h.

Scanning electron microscopy (SEM, Philips XL30-FEG) and high resolution transmission electron microscopy (HR-TEM, JEOL 2010F operating at 200 kV) were used to characterize the nanofillers. The powder samples were dispersed in isopropanol in an ultrasonic bath for 10 min before SEM and TEM observations. The TEM micrograph in Fig. 1 shows spherical Al_2O_3 particles of diameter ranging from 25 nm to 120 nm. Fig. 2 shows that the nanoclay exhibits a fibre-like amorphous structure in the as-received state and becomes a 3-D bundled rod-structure after heat treatment at 850 °C for 2 h.[11] The diffraction spots of the selected area electron diffraction pattern reveal the nanocrystalline nature of the heat-treated clay as shown by the inset in Fig. 2(b).

Micro-hardness (Vickers) tests were performed, with the measured hardness averaged from at least five indentation tests. The indentation load was fixed at 245 mN and held for 20 s for

[a]*Department of Mechanical Engineering, School of Engineering and Physical Sciences, Heriot-Watt University, Edinburgh, UK EH14 4AS. E-mail: R.Y.Fu@hw.ac.uk*
[b]*Centre for Materials Research & Innovation, University of Bolton, Bolton, UK BL3 5AB*
[c]*School of Mechanical and Aerospace Engineering, Nanyang Technological University, 50 Nanyang Avenue, Singapore 639798*
[d]*Department of Applied Physics, The Netherlands Materials Innovation Institute, University of Groningen, Nijenborgh 4, 9747 AG Groningen, The Netherlands*
† This paper is part of a *Journal of Materials Chemistry* themed issue on Actively Moving Polymers. Guest editor: Andreas Lendlein.

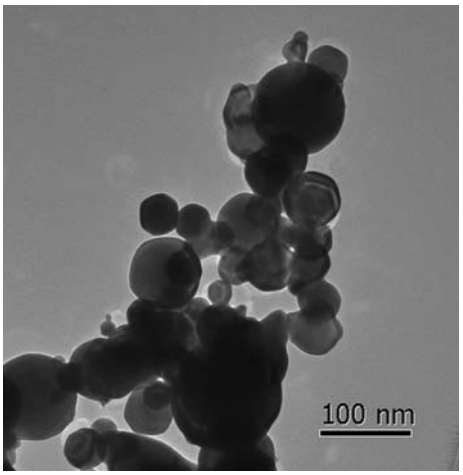

Fig. 1 TEM micrograph showing the morphology of Al_2O_3 nanoparticles.

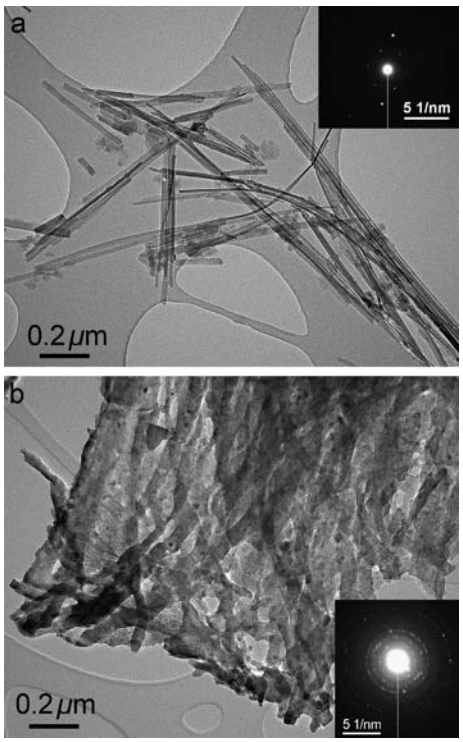

Fig. 2 TEM micrograph of as-received (a) and heat-treated (b) clay powders, with selected area diffraction pattern shown in the inset.

each test. Differential scanning calorimetry (DSC) analysis was performed using a Thermal Advantage DSC 2010 at a heating rate of 10 °C min^{-1} under a constant nitrogen flow. Dynamic mechanical thermal analyses (DMTA) were carried out in tensile mode with a TA Instruments DMA 2980 at a frequency of 1 Hz, a heating rate of 2 °C min^{-1} and a temperature range from 25 to 120 °C. Tensile tests were carried out using an Instron universal tensile instrument (Instron 5567) at a constant crosshead speed of 5 mm min^{-1} at room temperature (~20 °C). The experimental set-up and dimensions of the specimens followed British Standards (*BS ISO 20753:2008* Plastics—Test specimens, *BS EN ISO 527-1:1996* Plastics—Determination of tensile properties: Part 1 and *BS EN ISO 527-5:2009* Plastics—Determination of tensile properties: Part 5). Thermo-mechanical cyclic tests (one cycle of which is shown schematically in Fig. 3) were also performed to investigate the shape memory effect of the SMP and nanocomposites. These tests consisted of loading the specimen to a strain (ε_m) at a constant crosshead speed of 5 mm min^{-1} at a temperature T_{high} (stage 1), and then cooling down to the temperature T_{low} while holding the same strain ε_m (stage 2). After 5 min at the temperature T_{low}, the specimen was unloaded

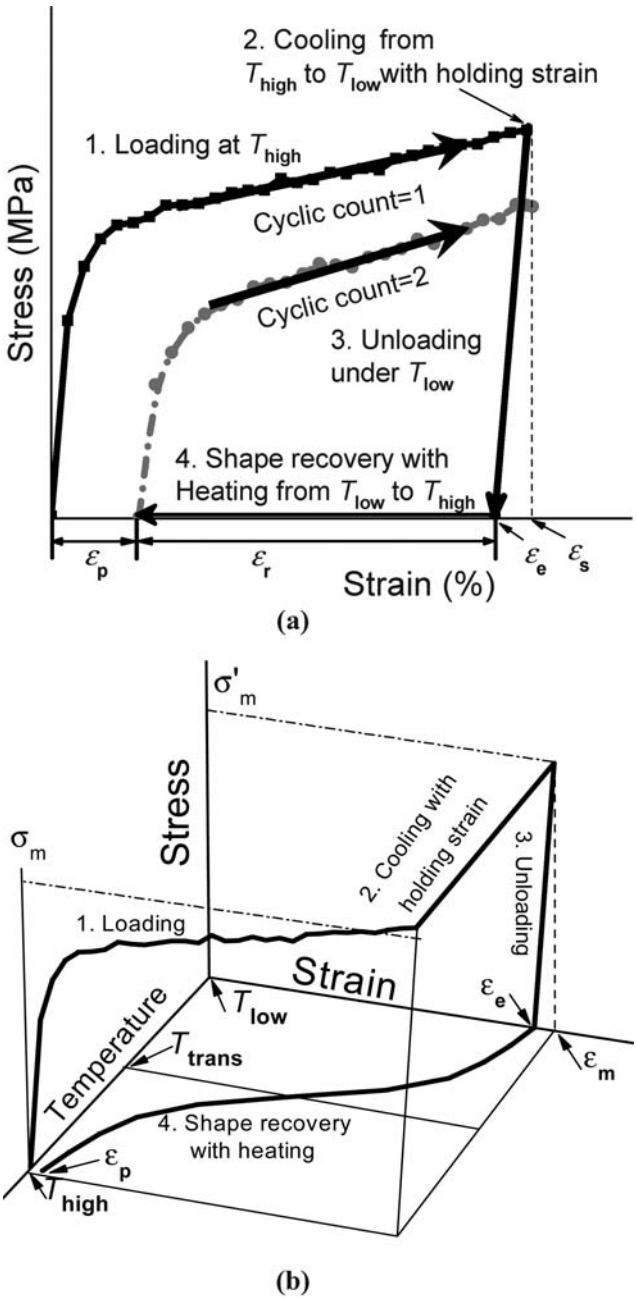

Fig. 3 Schematic drawings of cyclic tensile testing: (a) 2-D and (b) 3-D, There are four steps in each cycle: (1) stretching to ε_m at T_{high}; (2) cooling to T_{low} with holding strain; (3) Unloading and keeping shape at T_{low}; (4) heating up to T_{high}; then start of next cycle.

(stage 3) and reached a strain ε_e. The unloaded specimen was immediately heated from T_{low} to T_{high} in 5 min (stage 4), which left a permanent strain ε_p. This four-stage thermo-mechanical cycle was repeated for a total of 4 cycles. The fixed conditions of the cyclic test were: $\varepsilon_m = 100\%$; $T_{high} = 60\ ^\circ C$, and $T_{low} = 20\ ^\circ C$, and ε_e (the strain after unloading) and ε_p (the permanent strain) were both recorded for each specimen.

3. Results

3.1 Mechanical properties

Fig. 4(a) shows the recorded Vickers hardness for the three nanocomposites as a function of nanofiller content. Clearly, a significant increase in hardness was observed with the addition of the nanoparticles. With the addition of 4 wt% of the nanoclay powder, the microhardness reaches a maximum value of about 75 MPa, which is nearly 400% improvement compared to that of the pure PS. The Al_2O_3 nanoparticles show similar hardness enhancement as the nanoclay; whereas the SiO_2 nanoparticles demonstrate the weakest enhancement effect: the hardness is only doubled when the SiO_2 content reaches 4 wt%. It is also noticeable that the hardening effect is greatest for the first 0.5 wt% addition and is approximately the same for all three reinforcement materials thereafter.

Composites with 1 wt% nanofillers were selected for tensile tests to compare their stress–strain behaviour at room temperature (20 °C), typical stress–strain curves are shown in Fig. 4(b). From the maximum stress and strain results shown in Fig. 4(c), the SiO_2/PS composites show a nearly 16% increase in the maximum strength, and the Al_2O_3/PS and clay/PS composites present a much better enhancement, reflecting the hardness results. The Young's moduli (shown in Fig. 4(d)) measured from the tensile tests confirm that the clay/PS composites gave rise to the best enhancement, nearly 300% of the pure PS.

Fig. 5 shows the stress–strain behaviour of the clay/PS nanocomposite SMP as a function of clay content at room temperature. The tensile stress increases significantly with increasing clay content up to 1 wt%, and then decreases upon further addition of nanoclay. For example, incorporation of only 1 wt% clay results in a modulus that is almost three times as high as that of pure PS. The decrease in this enhancement effect after adding more than 1 wt% clay is likely due to an imperfect organic–inorganic interface and agglomeration of nanoparticles.[12,16]

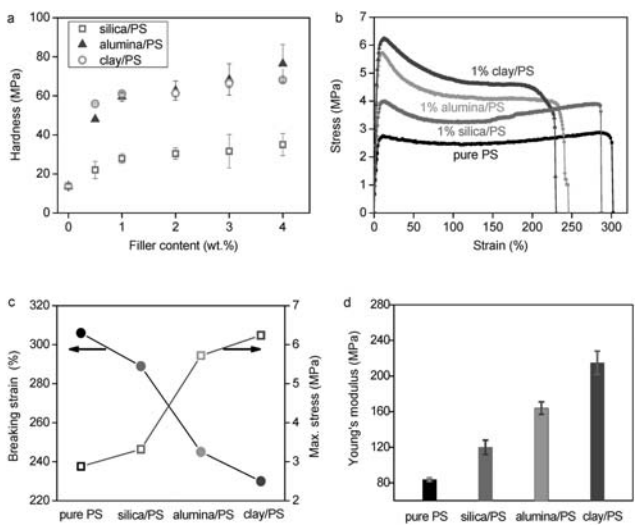

Fig. 4 Comparison of mechanical properties for nanocomposite SMP: (a) Vicker's hardness results with 25 g load and 20 s load time; (b) tensile results at room temperature; (c) breaking strain and maximum stress; (d) typical Young's modulus values from tensile test.

3.2 Thermal properties

DSC results in Fig. 6(a) reveal that, with the addition of all types of nanoparticles from 1 to 3 wt%, the glass transition temperatures decrease slightly (by less than 3 °C). Homogenous dispersion of nanoparticles in the polymer matrix is difficult to achieve without additional treatment of the fillers.[13,14] Aggregation of

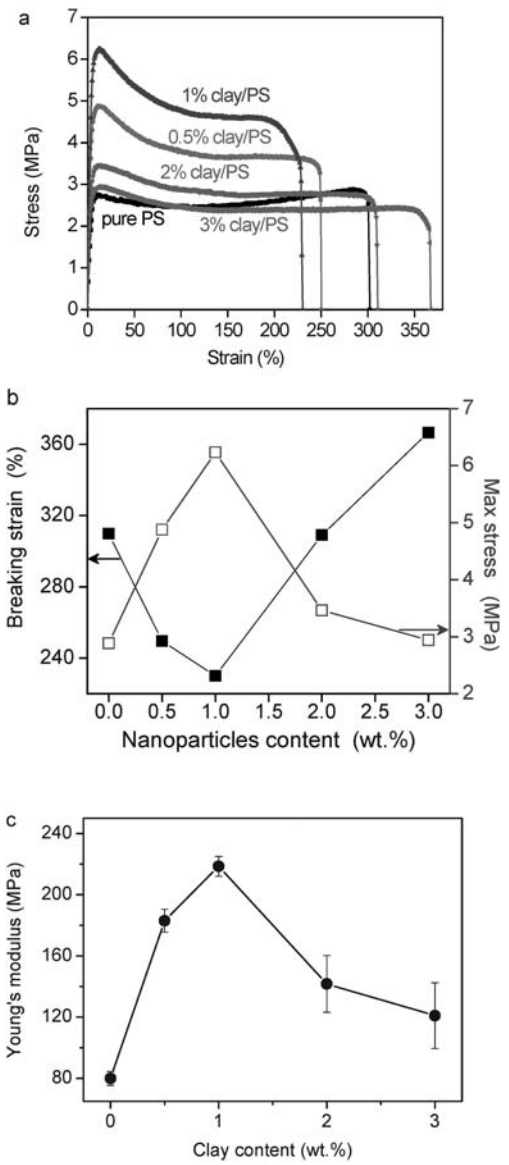

Fig. 5 Tensile results for nanocomposites of clay/PS: (a) typical stress–strain curve; (b) breaking strain and maximum stress; (c) Young's modulus as a function of clay content.

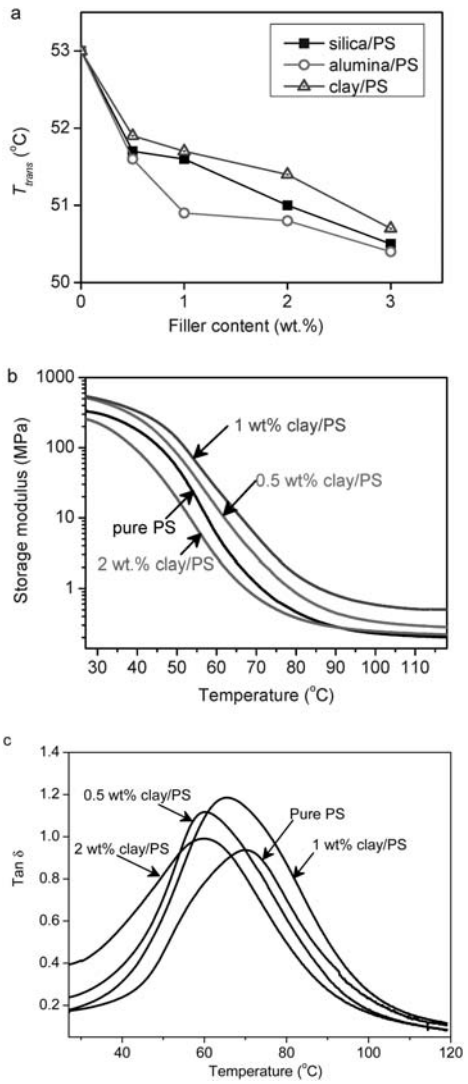

Fig. 6 Thermal property investigation on T_{trans} of nanoclay-based SMP composites (a) DSC results; (b) storage modulus *versus* temperature curves; (c) tan δ *versus* temperature results.

nanofillers in the nanocomposites was reported to cause some negative effects, such as a slight decrease in the transition temperature.[15] The clay/PS composites showed the smallest decrease in the transition temperature of the nanocomposites studied.

The clay/PS samples were selected to investigate the dynamic mechanical properties of the nanocomposites using DMTA. Fig. 6(b) shows the storage modulus (E') for the composites with different clay contents. The storage modulus obtained from DMTA tests has a maximum value for the SMP nanocomposite with 1 wt% clay, indicating that the stiffness of 1 wt% clay/PS nanocomposite is the highest among all the tested samples. A sharp drop in modulus is observed above T_g within a narrow temperature range, which has been frequently reported.[16] The tan δ curves shown in Fig. 6(c) reveal that the transition temperatures of the nanocomposites slightly increase with addition of clay content, which reflects what was observed in the DSC analysis. The nanocomposite with 0.1 wt% clay also shows the highest tan δ value, which reveals the best energy absorption capacity among these samples.[17] The damping effect depends strongly on the hard segment content, crystallization of the soft segment and cross-linking rate.[18,19] The best damping effect was achieved with 1 wt% clay content, as the incorporation of nanofiller maximizes the hard segments' content. However, with 2 wt% addition of clay, due to the poor dispersion of nanofillers, the energy absorption during deformation has been reduced, thus leading to a reduction in the damping effect.

3.3 Thermo-mechanical cyclic results

When an external stress is applied to the SMP, soft/flexible segments will be preferentially extended in the stress direction relative to the hard/fixed segment. The SMP studied in this paper is a cross-linked polystyrene where both cross-linking and nanofiller particles act as the hard/fixed segment. The shape memory properties are normally evaluated in terms of percentage shape recovery.[20,21] As can be seen from Fig. 7, the maximum stress of pure PS (1.45 MPa) at 60 °C is about half of that at room temperature (Fig. 5(b)). A similar behavior is also observed in the nanocomposites. This can be understood by the chains of shape memory polymer becoming flexible above the transition temperature, which results in a reduction of the maximum stress. The maximum stress of 1 wt% clay/PS nanocomposite was the highest among all the samples, showing a good enhancement even at temperatures above T_{trans}. When the cyclic tensile process proceeds, the residual strain ε_p increases (see Fig. 7), which could be attributed to such possibilities as: (1) random breaking of covalent cross-link bonds, (2) energy storing by the fillers,[22] (3) a blocking effect by incorporated nanofillers,[12] *etc.*

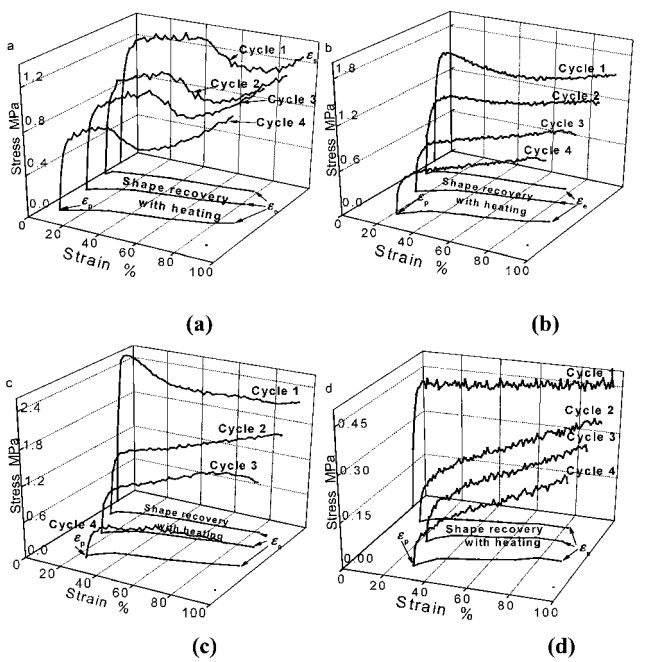

Fig. 7 Thermal mechanical cyclic testing results: (a) pure PS; (b) 0.5 wt% clay/PS composites; (c) 1 wt% clay/PS composites; (d) 2 wt% clay/PS composites.

The shape memory effect can be quantified using the strain recovery ratio as a function of cycle number N, defined by eqn (1):[20]

$$R_r(N) = \frac{\varepsilon_e(N) - \varepsilon_p(N)}{\varepsilon_e\ (N) - \varepsilon_p(N-1)} \quad (1)$$

where $R_r(N)$ is the strain recovery ratio in the cycle number N, $\varepsilon_e(N)$ is the unloading strain at T_{low} in the cycle number N, $\varepsilon_p(N)$ and $\varepsilon_p(N-1)$ are residual strains at cycle number N and $N-1$, respectively. Fig. 8 summarizes the recovery ratio of the clay/PS composite SMPs for the cyclic tests. It has been found that the recovery rates of all the samples are above 85%. The recovery ratio for 2 wt% clay nanocomposite is nearly 15% lower than that of the pure PS, and this can be attributed to significant agglomeration of nanofillers in the polymer, and random breaking of covalent cross-link bonds. There seems to be a slight decrease in the recovery rate with cycle numbers, but then a slight increase after two or three cycles. This is a typical "learning phase" seen in many shape-memory polymers.[4,6] After the first tensile cycle, some of the cross-link points will break in the SMP and composites, which could freeze the free movement of the molecular chain, thus causing the reduction in the recovery rate. The recovery strain becomes stable as more molecular chains function as the soft segment, leading to an increase in the reversible recovery rate.

3.4 Shape memory recovery

SMP and nanocomposite samples with a thickness of 0.6 mm and width of 10 mm were rolled after heating to 90 °C, and kept the shape fixed during cooling to room temperature (20 °C). The shape recovery test was carried out in hot water at 60 °C. The pure PS sample (see Fig. 9) exhibited a prompt response in hot water and almost reached 90% recovery within 20 s. The nanocomposites also showed good shape memory recovery but with a faster recovery speed (recovering within 12 s) than that of the pure PS. The reason could be that the T_{trans} of the nanocomposite SMPs decreases with addition of nanoclay filler. As a further assessment of the capacity of the materials, a microgripper based on pure PS was manufactured using laser beam micromachining as shown in Fig. 10. A good shape recovery of

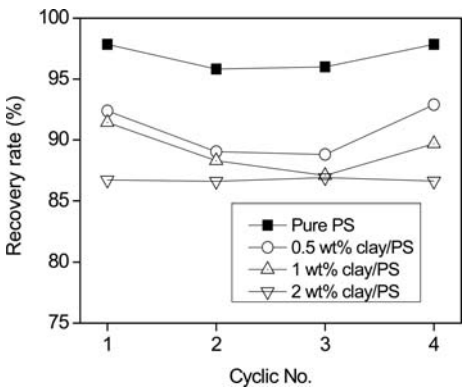

Fig. 8 Recovery rate *versus* cyclic number of pure PS and clay/PS samples.

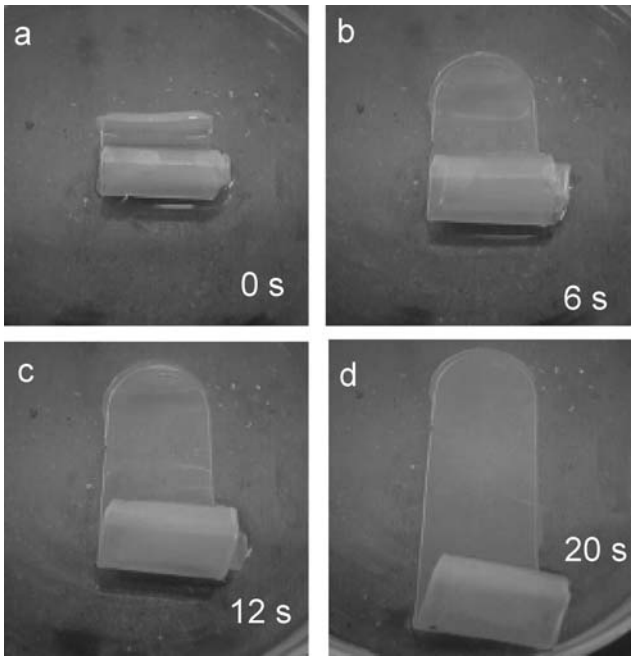

Fig. 9 Recovery of a pure PS SMP sheet in 60 °C hot water.

the gripper at 80 °C was demonstrated. A five penny coin was used as a comparison of the dimension changing. The demonstration of the SMP microgripper shows a potential biomedical or microassembly application.

4. Discussion

Generally, when nanofillers with high modulus are added into a lower modulus polymer matrix, the modulus and strength of the nanocomposites will be enhanced through an improved load transfer from the matrix to the filler. Fig. 11 illustrates the microstructure of nanofillers in a polymer matrix. Nanofillers dispersed in the polymer matrix reinforce the soft matrix through load transfer. When the aspect ratio of the particles equals unity (spherical nanoparticles), the composite modulus is dependent on a number of particle characteristics such as their modulus, density, the particle size and shape, the volume fraction, and the nature of the interface. As the modulus and density of Al_2O_3 is much larger than that of SiO_2, the enhancement effect for the Al_2O_3/PS sample is more significant, as shown in Fig. 4. The rod-like nanofillers may bridge more polymer chains and afford more effective load transfer, leading to an improvement in strength. Upon adding a critical volume fraction of nanorods (such as nanoclay), the nanorods stretch and perturb the polymer matrix, and the polymer blend confines the nanorods, generating elongated domains that are reinforced by these fillers.[23] Nanofillers with rod-like structures, as compared with spherical nanoparticles, have been predicted to be better in homopolymer systems because the stress concentration was reduced, and the stress was transferred by the high aspect ratio and specific geometry of the fillers.[24] In this study, the remarkable improvement of mechanical properties of SMPs reinforced with 1 wt% clay in comparison with other spherical fillers (see Fig. 4) confirms this prediction.

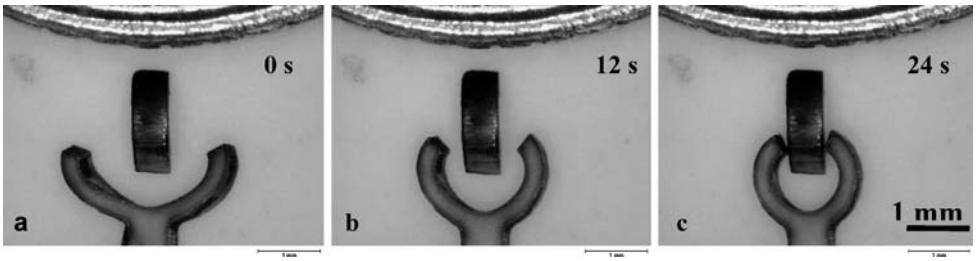

Fig. 10 Shape recovery of a micro-gripper based on a pure PS copolymer (the edge of a five pence coin is also shown for comparison).

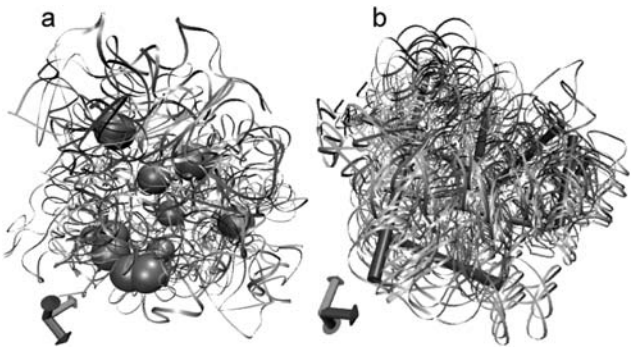

Fig. 11 3-D schematic demonstration of nanocomposite systems: (a) with spherical fillers (such as Al_2O_3 and SiO_2), (b) with rod-like filler (such as clay or carbon nanotubes).

Many empirical or semi-empirical equations have been proposed to predict the modulus of composites. Einstein gave a simple equation to predict the Young's modulus of composites reinforced with rigid particles:[25]

$$\frac{E}{E_m} = 1 + 2.5\phi_f \tag{2}$$

where E and E_m represent the Young's modulus of the composite and matrix, ϕ_f is the volume fraction of filler (vol%). Einstein's equation is applicable only at low concentrations of filler and assumes perfect interface combination between filler and matrix, as well as perfect dispersion of individual filler particles.[26] Halpin and Tsai[27,28] proposed a similar analytical equation, adapted for a variety of reinforcement geometries, including discontinuous filler reinforcement:

$$\frac{E}{E_m} = \frac{1 + \zeta\eta\phi_f}{1 - \eta\phi_f} \tag{3}$$

where ζ is a shape parameter, decided by filler geometry and loading direction, and η is given by:

$$\eta = \frac{E_f/E_m - 1}{E_f/E_m - 1 + \zeta} \tag{4}$$

where E_f is the Young's modulus of the filler. Following Halpin and Kardos,[27] a shape parameter based on aspect ratio $\zeta = 2\,(l/d)$ will be used in this study.

Mori and Tanaka considered the effect of an infinite volume fraction of inclusions in an aligned short-fiber composite in their models.[29–31] Tandon and Weng[31] have derived comprehensive analytical expressions for the elastic modulus of an isotropic matrix filled with spheroidal and unidirectionally aligned non-spherical inclusions. The longitudinal (along the inclusion alignment direction) and transverse elastic moduli can be generated through examining the influence of aspect ratio, from zero to infinity, on the offload transfer in a transversely isotropic composite:[29]

$$\frac{E_{11}}{E_m} = \frac{A}{A + \phi_f(A_1 + 2\upsilon_m A_2)} \tag{5}$$

$$\frac{E_{22}}{E_m} = \frac{2A}{2A + \phi_f(-2\upsilon_0 A_3 + (1 - \upsilon_m)A_4 + (1 + \upsilon_m)A_5 A)} \tag{6}$$

where E_{11} is the longitudinal modulus and E_{22} is the transverse modulus, υ_0 is the Poisson's ratio of the matrix, A_1, A_2, A_3, A_4, A_5, and A are functions of the Eshelby's tensor, related to the properties of the filler and the matrix.[26] Eqn (5) and (6) account of the effect of filler shape, for example, rod-like, plate-like, or disc-like, *etc.* Given that nanofillers are rarely aligned, Fornes *et al.*[32] suggested equations for random orientation in all three orthogonal directions:

$$E_{ran-3D}^{fibers} = 0.184E_{11} + 0.816E_{22} \tag{7}$$

$$E_{ran-3D}^{plateles} = 0.49E_{11} + 0.51E_{22} \tag{8}$$

Fig. 12 compares the calculated and measured moduli for the SMPs studied. Two models, the Halpin–Tsai model and the Mori–Tanaka model, were used to calculate the reinforcement. The Halpin–Tsai model considerably over-estimates the effect of silica reinforcement and under-estimates a little the effect of clay reinforcement. The Mori–Tanaka model predicts the observed ranking of the three fillers, but over-estimates all of the effects. The better performance of the Mori–Tanaka model is attributed

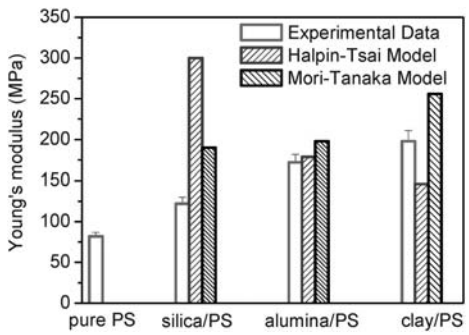

Fig. 12 Comparison of predicted Young's modulus with experimentally measured data for 0.5 wt% fillers/PS nanocomposite SMPs.

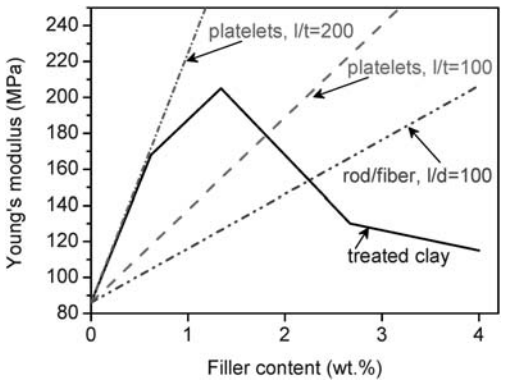

Fig. 13 Prediction of Young's modulus of nanocomposite SMPs *versus* experimental data.

to its considering the sample expansion and the effect of an infinite volume fraction of inclusions. The considerable difference between the calculated and measured Young's modulus for silica/PS composites may be attributed to the agglomeration of nanofillers caused by the surface hydro-groups, an effect that has been observed by others in nano-SiO_2.[33,34]

Fig. 13 shows calculated results of Young's modulus of composites with different shapes of fillers based on eqn (7) and (8) (Mori–Tanaka model). Of the three forms considered, platelet fillers are more effective, even for the same aspect ratio, as the platelet filler shows the ideal reinforcement because of its high aspect ratio and multi-direction load transfer ability.[23,32] The experimental results (average data only) for the treated clay follow a similar trend to the high aspect ratio platelets model for low filler contents, consistent with the TEM observation in Fig. 2b, where the rod-like clay forms a more plate-like structure after heat treatment. The deviation from the predicted curve at higher filler contents (beyond 1 wt%) may be due to increased agglomeration during fabrication of the nanocomposites.

5. Conclusion

Thermo-mechanical properties of the PS-based nanocomposites were studied. Nanofillers exhibit an effective enhancement in the strength and modulus of composite SMPs, at the expense of slightly reduced recovery rate. Among the three types of nanofiller, the heat-treated nanoclay achieved the best improvement in strength. DMTA results indicated that the 1 wt% clay composites had the highest storage modulus and the best energy absorption capacity. Thermal cyclic tests indicated that the recovery rates of all the nanocomposite SMPs are above 85%, and good shape recovery ability was demonstrated. Two theoretical models were adopted to evaluate the reinforcement effects, and the analysis results revealed that the Mori–Tanaka model provides a better description by taking into account the influence of the aspect ratio of nanofillers on thermo-mechanical properties, such as Young's moduli of composite SMPs.

Acknowledgements

We thank Prof. D. Hand, Dr P. Jonathan, Steven Fuhrmann and Mr W. L. Chang for their experimental help and the Carnegie Trust for financial support. The nanoclay was kindly provided by Prof. G. H. Pan from the Southeast University, China. W. M Huang would like to acknowledge the support from A*STAR, Singapore (SERC No: 092 137 0016).

References

1 B. S. Lee, B. C. Chun, Y. C. Chuang, K. I. Sul and J. W. Chos, *Macromolecules*, 2001, **34**, 6431.
2 N. G. Sahoo, Y. C. Jung, H. J. Yoo and J. W. Cho, *Compos. Sci. Technol.*, 2007, **67**, 1920.
3 R. Mohr, K. Kratz, T. Weigel, M. Lucka-Gabor, M. Moneke and A. Lendlein, *Proc. Natl. Acad. Sci. U. S. A.*, 2006, **103**, 3540.
4 A. Lendlein, H. Jiang, O. Jünger and R. Langer, *Nature*, 2005, **434**, 879.
5 S. Hayashi, S. Kondo, P. Kapadia and E. Ushioda, *Plast. Eng.*, 1995, **51**, 29.
6 M. Behl and A. Lendlein, *Mater. Today*, 2007, **10**, 20.
7 C. Liang, C. A. Rogers and E. Malafeew, *J. Intell. Mater. Syst. Struct.*, 1997, **8**, 380.
8 K. Gall, M. L. Dunn, Y. P. Liu, D. Finch, M. Lake and N. A. Munshi, *Acta. Mater.*, 2002, **50**, 5115.
9 K. Sakurai, Y. Shirakawa, T. Kashiwagi and T. Takahashi, *Polymer*, 1994, **35**, 4238.
10 F. Li and R. C. Larock, *Biomacromolecules*, 2003, **4**, 1018.
11 B. Xu, W. M. Huang, Y. T. Pei, Z. G. Chen, A. Kraft, R. Reuben, J. Th. M. De Hosson and Y. Q. Fu, *Eur. Polym. J.*, 2009, **45**, 1904.
12 H. Fischer, *Mater. Sci. Eng., C*, 2003, **23**, 763.
13 H. Tobushi, T. Hashimoto, N. Ito, S. Hayashi and E. Yamada, *J. Intell. Mater. Syst. Struct.*, 1998, **9**, 127.
14 Q. H. Meng, J. L. Hu and S. Mondal, *J. Membr. Sci.*, 2008, **319**, 102.
15 C. D. Liu, S. B. Chun, P. T. Mather, L. Zhang, E. H. Haley and E. B. Coughlin, *Macromolecules*, 2002, **35**, 9868.
16 B. K. Kim, Y. J. Shin, S. M. Cho and H. M. Jeong, *J. Polym. Sci., Part B: Polym. Phys.*, 2000, **38**, 2652.
17 B. S. Lee, B. C. Chun, Y. C. Chung, K. I. Sul and J. W. Chos, *Macromolecules*, 2001, **34**, 6431.
18 T. Takahashi, N. Hayashi and S. Hayashi, *J. Appl. Polym. Sci.*, 1996, **60**, 1061.
19 P. Pissis, L. Apekis, C. Christtodoulides, M. Niaounakis, A. Kyritsis and J. Nedbal, *J. Polym. Sci., Part B: Polym. Phys.*, 1996, **34**, 1529.
20 Q. Q. Ni, C. S. Zhang, Y. Fu, G. Dai and T. Kimura, *Compos. Struct.*, 2007, **81**, 176.
21 J. D. Merline, C. P. Reghunadhan, C. Gouri, R. Sadhana and K. N. Ninan, *Eur. Polym. J.*, 2007, **43**, 3629.
22 Q. H. Meng, J. L. Hu and Y. Zhu, *J. Appl. Polym. Sci.*, 2007, **106**, 837.
23 G. A. Buxton and A. C. Balazs, *Mol. Simul.*, 2004, **30**, 249.
24 G. A. Buxton and A. C. Balazs, *J. Chem. Phys.*, 2002, **117**, 7649.
25 A. Einstein, *Ann. Phys. (Leipzig)*, 1905, **17**, 549.
26 C. H. Hsueh and P. F. Becher, *J. Am. Ceram. Soc.*, 2005, **88**, 1046.
27 J. C. Halpin, *Compos. Mater.*, 1969, **3**, 732.
28 J. C. Halpin and J. L. Kardos, *Polym. Eng. Sci.*, 1976, **16**, 344.
29 T. Mori and K. Tanaka, *Acta Metall.*, 1973, **21**, 571.
30 C. H. Hsueh, *J. Am. Ceram. Soc.*, 1989, **72**, 344.
31 G. P. Tandon and G. J. Weng, *Polym. Compos.*, 1984, **5**, 327.
32 T. D. Fornes, P. J. Yoon, D. L. Hunter, H. Keskkula and D. R. Paul, *Polymer*, 2002, **43**, 5915.
33 M. Z. Rong, M. Q. Zhang, S. L. Pan, B. Lehmann and K. Friedrich, *Polym. Int.*, 2004, **53**, 176.
34 S. Gupta, Q. L. Zhang, T. Emrick, A. C. Balazs and T. P. Russell, *Nat. Mater.*, 2006, **5**, 229.

